Structure
Article

Structure and Rearrangements in the Carboxy-Terminal Region of SpIH Channels

Galen E. Flynn,[1] Kevin D. Black,[1] Leon D. Islas,[1,3] Banumathi Sankaran,[2] and William N. Zagotta[1,*]
[1] Department of Physiology and Biophysics, Howard Hughes Medical Institute, University of Washington, Seattle, WA 98195, USA
[2] Advanced Light Source, Lawrence Berkeley National Laboratory, Berkeley, CA 94720, USA
[3] Present address: Departamento de Fisiologia, Facultad de Medicina, Universidad Nacional Autonoma de Mexico, Mexico, D.F. Mexico CP 04510.
*Correspondence: zagotta@u.washington.edu
DOI 10.1016/j.str.2007.04.008

SUMMARY

Hyperpolarization-activated cyclic nucleotide-modulated (HCN) ion channels regulate the spontaneous firing activity and electrical excitability of many cardiac and neuronal cells. The modulation of HCN channel opening by the direct binding of cAMP underlies many physiological processes such as the autonomic regulation of the heart rate. Here we use a combination of X-ray crystallography and electrophysiology to study the allosteric mechanism for cAMP modulation of HCN channels. SpIH is an invertebrate HCN channel that is activated fully by cAMP, but only partially by cGMP. We exploited the partial agonist action of cGMP on SpIH to reveal the molecular mechanism for cGMP specificity of many cyclic nucleotide-regulated enzymes. Our results also elaborate a mechanism for the allosteric conformational change in the cyclic nucleotide-binding domain and a mechanism for partial agonist action. These mechanisms will likely extend to other cyclic nucleotide-regulated channels and enzymes as well.

INTRODUCTION

Cyclic nucleotides are ubiquitous intracellular second messengers that regulate a wide array of physiological processes including heart rate, retinal phototransduction, smooth muscle tone, and sperm chemotaxis. This regulation by cyclic nucleotides is carried out by direct binding to a variety of effector proteins including protein kinases, ion channels, transcription factors, and guanine nucleotide exchange proteins. Changes in cyclic nucleotide levels often regulate only specific pathways inside the cell. This specificity arises in part from selectivity of these effector proteins for either cAMP or cGMP. However, the molecular mechanism for the cyclic nucleotide specificity of these two closely related cyclic nucleotides remains unknown, partially because of the absence of a high-resolution structure of a cGMP-specific effector protein.

To better understand the mechanisms for cyclic nucleotide activation and selectivity in these effector proteins, we studied hyperpolarization-activated cyclic nucleotide-modulated (HCN) ion channels. HCN channels are weakly potassium-selective cation channels that open their transmembrane pore in response to both membrane hyperpolarization and the direct binding of cyclic nucleotides. HCN channel activation by membrane hyperpolarization gives rise to a resting current that controls the resting membrane potential and dendritic integration, and to a pacemaker current that promotes the spontaneous rhythmic firing of action potentials in nerve and cardiac cells (Baruscotti and Difrancesco, 2004; Biel et al., 2002; Pape, 1996; Robinson and Siegelbaum, 2003). The cyclic nucleotide-dependent modulation of the HCN channels can regulate cellular excitability and is thought to underlie the autonomic regulation of the heart rate (DiFrancesco, 1991; DiFrancesco et al., 1989).

HCN channels are members of the voltage-activated family of ion channel proteins (Craven and Zagotta, 2004). Like most voltage-activated channels, they are composed of four subunits, each of which contains six transmembrane segments (S1–S6) and intracellular amino and carboxyl termini. HCN channels belong to a specialized subfamily of voltage-activated channels called cyclic nucleotide-regulated channels that also include cyclic nucleotide-gated (CNG) channels and ether-a-go-go (*eag*)-like channels. This subfamily contains a highly conserved carboxy-terminal region that is composed of a cyclic nucleotide-binding domain (CNBD) and a C-linker region that connects the CNBD of each subunit to the pore-forming transmembrane segment S6. An X-ray crystal structure of the HCN2 carboxy-terminal region revealed a four-fold symmetric gating ring formed by the C linker and CNBD of four subunits (Zagotta et al., 2003). In both HCN channels and CNG channels, intracellular cyclic nucleotides bind directly to the CNBD of each subunit, producing an allosteric conformational change that increases the open probability of the channel pore.

In contrast to the mammalian HCN channels, an HCN channel from sea urchin sperm has very different properties (Gauss et al., 1998). This channel, called SpIH or SpIH1, is 34% identical overall to HCN2, with 59.4% identity in its carboxy-terminal region. Whereas cGMP is a full agonist for HCN2 channels, cGMP is a partial agonist for

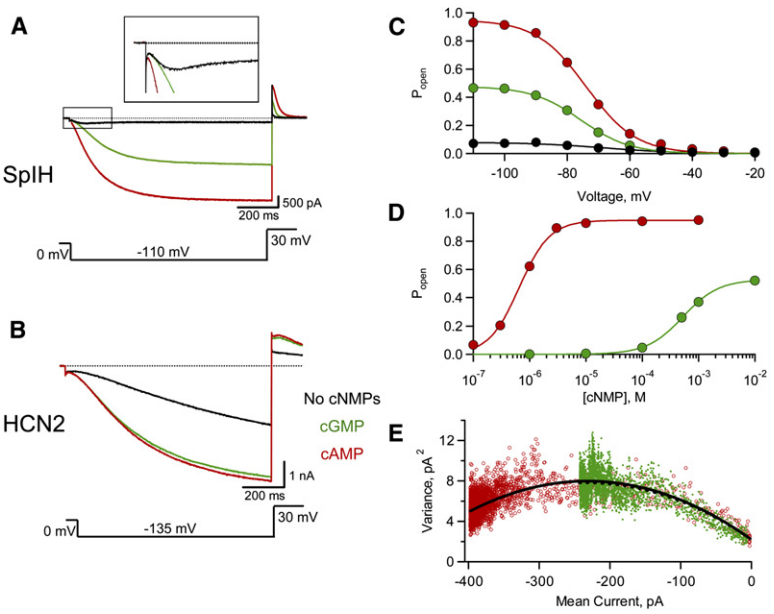

Figure 1. cGMP Is a Partial Agonist on SpIH Channels

(A and B) Currents from SpIH (A) or HCN2 (B) channels recorded in the inside-out configuration in the absence of cyclic nucleotide (black) or the presence of 1 mM cAMP (red) or 10 mM cGMP (green). Voltage steps to −110 mV or −135 mV were applied respectively, followed by steps to +30 mV.

(C) Voltage dependence of SpIH channels. Open probabilities calculated from tail current measurements and nonstationary noise analysis (see Experimental Procedures) are shown for channels in the same patch in the absence (black) or presence of cAMP (red) or cGMP (green). The smooth lines are fits of the Boltzmann function to the data. For this patch, in the absence of cNMP, $V_{1/2}$ = −67.8 mV and $z\delta$ = 2.1; in cAMP, $V_{1/2}$ = −73.9 mV and $z\delta$ = 3.2; and in cGMP, $V_{1/2}$ = −75.6 mV and $z\delta$ = 3.3.

(D) Dose-response relationships for SpIH channels. Open probabilities are shown for different concentrations of cAMP (red) and cGMP (green) and fit by a Hill equation. For this patch, cAMP had a $K_{1/2}$ = 659 nM and a Hill Coef = 1.6, while cGMP had a $K_{1/2}$ = 526 μM and a Hill Coef = 1.35.

(E) Nonstationary noise analysis of SpIH channels recorded at −130 mV in the presence of 1 mM cAMP (red) or 1 mM cGMP (green). Mean current-variance relationships were fit with a hyperbolic function to determine the number of channels and single-channel conductance. For this patch, the maximum current in saturating cAMP at −130 mV was −397 pA, the Po = 0.85, and the single-channel conductance was 0.385 pS. The maximum current in saturating cGMP at −130 mV was −242 pA, the Po = 0.54, and the single channel conductance was 0.371 pS.

SpIH channels (Kaupp and Seifert, 2001): saturating concentrations of cGMP produce smaller currents than saturating concentrations of cAMP. Activation of the channels can be modeled as two coupled transitions: binding of the agonists to the closed state of the channel, and an allosteric conformational change, coupled to agonist binding, that opens the channel pore (Altomare et al., 2001; Craven and Zagotta, 2004; Monod et al., 1965). Agonist specificity could arise from either tighter binding of the agonist or more favorable opening by the bound agonist (or both). Partial agonism results from the inability of the bound agonist to fully promote channel opening (Del Castillo and Katz, 1957; Li et al., 1997). The discovery of a partial agonist on SpIH channels allows us to separate the binding transitions from the opening transitions and to probe the molecular nature of the cyclic nucleotide specificity of SpIH channels.

Whereas no cGMP-specific effector protein structures have yet been solved, two classes of models have been proposed for cGMP specificity based on the cAMP-bound structures of catabolite gene activator protein (CAP) (Weber et al., 1987) and the regulatory subunit of the cAMP-dependent protein kinase (Su et al., 1995). In these structures, cAMP is bound at the interface between a β roll and an α helix (C helix). In model 1 (see below), cGMP specificity arises from interactions between a threonine in the β roll and the N2 amine of cGMP (Altenhofen et al., 1991; Kumar and Weber, 1992; Scott et al., 1996; Weber et al., 1989). This interaction could only occur if bound cGMP were in the *syn* configuration, where a C1-N9 bond rotation places the guanine ring near the ribose moiety. In model 2 (see below), cGMP specificity arises from interactions between an aspartate in the C helix and the N1 and N2 nitrogens of cGMP (Varnum et al., 1995). Based on modeling using the structure of CAP, this interaction was thought to only occur if bound cGMP was in the *anti* configuration, where a C1-N9 bond rotation moves the guanine ring away from the ribose moiety.

Here, using a combination of X-ray crystallography and electrophysiology, we show that the mechanism for cGMP specificity is a composite of the two models (model 3; see below). cGMP is held in the *syn* configuration by interactions with a threonine in the β roll, but this interaction is not sufficient to promote channel opening by cGMP. Instead, specific interactions with an aspartate in the C helix promote channel opening by cGMP. This mechanism likely underlies the cGMP specificity of CNG channels and cGMP-dependent protein kinases as well. Furthermore, our results support a specific model for an allosteric conformational change in the CNBD and elucidate the mechanism of partial agonist action for cGMP on SpIH channels.

RESULTS

The behavior of SpIH channels is different from that of HCN channels (Gauss et al., 1998). Currents from inside-out patches were recorded from *Xenopus* oocytes expressing either SpIH channels or HCN2 channels. In the absence of cyclic nucleotides, HCN2 channels were opened substantially by hyperpolarizing pulses alone, whereas

Table 1. Comparison of the Voltage Dependence of Wild-Type and Mutant SpIH Channels at Saturating Ligand Concentrations

	cAMP		cGMP		No cNMPs		
Channel	$V_{1/2}$ (mV)	zδ	$V_{1/2}$ (mV)	zδ	$V_{1/2}$ (mV)	zδ	n
SpIH	−72.3 ± 1.2	3.4 ± 0.16	−74.1 ± 1.4	3.7 ± 0.21	−66.8 ± 2.4	2.1 ± 0.12	8
V621T	−79.2 ± 2.2	3.8 ± 0.16	−80.9 ± 2.1	3.7 ± 0.32	−76.6 ± 2.8	1.8 ± 0.37	6
I665D	−74.5 ± 2.1	4.5 ± 0.21	−76.6 ± 3.6	2.4 ± 0.29	−72.2 ± 2.4	1.6 ± 0.20	6
V621T,I665D	−81.5 ± 1.1	4.1 ± 0.43	−82.4 ± 1.7	3.9 ± 0.35	−77.8 ± 1.7	1.6 ± 0.28	6

SpIH channels produced only small, rapidly inactivating currents (Figures 1A and 1B, black traces). Application of cAMP to these inside-out patches caused an increase in the current for both channels (Figures 1A and 1B, red traces). This increase, however, was larger for SpIH channels, where it was produced by a removal of inactivation with little or no shift in voltage dependence (Figure 1C; Table 1) (Shin et al., 2004). In addition, unlike on HCN2 channels, cGMP behaves as a partial agonist on SpIH channels (Figures 1A and 1B, green trace versus red trace). At hyperpolarized voltages, saturating concentrations of cGMP activated only half of the current activated by cAMP (I_{cGMP}/I_{cAMP} = 0.51 ± 0.035, n = 8). Furthermore, the apparent affinity of SpIH channels was almost three orders of magnitude larger for cAMP (0.72 ± 0.04 μM, n = 8) than for cGMP (479 ± 58.5 μM, n = 8) (Figure 1D; Table 2). The difference between the amount of current elicited by saturating cGMP relative to cAMP reflects a difference in open probability for the two ligands and not a difference in single-channel conductance, as determined by nonstationary noise analysis (Figure 1E; Table 3). These results indicate that, in SpIH channels, cGMP is a true partial agonist, able to bind to channels but unable to fully promote opening.

Structure of the Carboxy-Terminal Domain of SpIH

To determine why cGMP is not a full agonist on SpIH channels, we turned to X-ray crystallography. A carboxy-terminal fragment of SpIH, containing the C linker (residues 471–550) and CNBD (residues 551–665), was cocrystallized with cAMP, and the structure was solved by molecular replacement to 1.9 Å resolution (Figure 2; Table 4; see Table S1 in the Supplemental Data available with this article online). Like the HCN2 carboxy-terminal region (Zagotta et al., 2003), the SpIH fragment assembled as a four-fold symmetric tetramer (Figure 2). The C-linker region of each subunit is predicted to be situated closest to the membrane and is composed of six α helices, designated A′–F′ (Figure 3A). This region from each subunit assembled to form a tetrameric "gating ring" that would be just below and concentric with the channel pore. Interactions between neighboring C-linker regions constitute virtually all of the intersubunit interactions in the tetramer, burying 2876 $Å^2$ of solvent-accessible surface area. Hanging below each C linker was a CNBD, composed of an eight-stranded β roll and four α helices (A, B, P, and C) (Figure 3A). Despite the functional differences between SpIH and HCN2, the SpIH structure has a very similar folding pattern to the previously solved structure of the HCN2 carboxy-terminal region (Zagotta et al., 2003) (root-mean-square deviation [rmsd] of the Cα atoms of 0.86 Å).

The CNBD of SpIH also shares substantial similarity with the CNBD of HCN2 and other CNBD-containing proteins. As in HCN2 (Zagotta et al., 2003) and CAP (Weber et al., 1987), cAMP binds in the *anti* configuration in SpIH (Figure 3B), forming interactions with both the β roll and the C helix of the CNBD. This configuration is different from that observed in the regulatory subunit of the cAMP-dependent protein kinase, where cAMP is in the *syn* configuration (Su et al., 1995). In the SpIH crystal structure, the phosphoribose ring of cAMP interacted exclusively with the β roll through electrostatic and hydrogen-bonding interactions with residues G610, E611, I612, C613, R620, and V621 (Figure 3C). The adenine ring formed interactions with residues in both the β roll (I592, T601, and L603) and the C helix (R661 and I665). With the exception of V621 (see below), these ligand interactions are all similar or identical in the HCN2 structure.

To determine why cGMP is only a partial agonist on SpIH, we next attempted to crystallize the SpIH carboxy-terminal region with cGMP bound. However, despite repeated attempts with various conditions, we were

Table 2. Comparison of the Cyclic Nucleotide Dependence of Wild-Type and Mutant SpIH Channels at −100 mV

		cAMP		cGMP		
Channel	I_{cGMP}/I_{cAMP}	$K_{1/2}$ (μM)	Hill Coef	$K_{1/2}$ (μM)	Hill Coef	n
SpIH	0.51 ± 0.035	0.717 ± 0.04	1.78 ± 0.08	479 ± 59.5	1.44 ± 0.04	8
V621T	0.49 ± 0.025	1.07 ± 0.05	1.92 ± 0.06	34.2 ± 2.5	1.9 ± 0.17	6
I665D	0.09 ± 0.02	11.5 ± 0.81	2.28 ± 0.06	955 ± 420	0.92 ± 0.06	6
V621T,I665D	1.23 ± 0.06	32.3 ± 5.6	1.1 ± 0.007	4.3 ± 1.3	1.6 ± 0.14	6

Table 3. Comparison of Nonstationary Noise Analysis of Wild-Type and Mutant SpIH

Channel	cNMP	P_o, cNMP	γ, pS	n
SpIH	cAMP	0.92 ± 0.02	0.38 ± 0.006	5
V621T	cAMP	0.93 ± 0.02	0.55 ± 0.05	3
I665D	cAMP	0.83 ± 0.04	0.34 ± 0.02	3
V621T,I665D	cAMP	0.65	0.41	2
SpIH	cGMP	0.51	0.37	2
V621T,I665D	cGMP	0.84 ± 0.01	0.44 ± 0.02	3

unable to obtain cocrystals with cGMP, even with very high cGMP concentrations (>100 mM). Previously it has been shown that the tetramerizaton affinity of the HCN2 carboxy-terminal domain is dependent on the binding of cyclic nucleotide (Zagotta et al., 2003). The inability to cocrystallize with cGMP could result from a number of factors, including a different conformation of the protein, a difference in oligomerization, or protein inhomogeneity when cGMP is bound.

Mutations that Make cGMP a Full Agonist

If the reason that cGMP is not a full agonist is that it cannot completely stabilize the conformational change in the CNBD, one might expect protein inhomogeneity and difficulty in crystallization when cGMP is bound. We therefore turned to a different strategy to determine why cGMP is not a full agonist in SpIH: identifying mutations in the CNBD that convert cGMP into a full agonist and determining the structure of those mutants. As cGMP is a full agonist in HCN2 channels, we looked for differences in the structures of SpIH and HCN2. One notable difference is that a threonine in the β roll of HCN2 (T592) is a valine in SpIH (V621) (Figure S1). In the crystal structure of the HCN2 carboxy-terminal domain, this threonine forms a specific hydrogen bond with the N2 amine group of the guanine ring of cGMP (Zagotta et al., 2003). This hydrogen bond is only possible because the bound cGMP is in the *syn* configuration (whereas cAMP is in the *anti* configuration). Indeed, a threonine is present at this position in virtually all cGMP-regulated enzymes including CNG channels and cGMP-dependent protein kinases (Figure S1), and has been proposed to be important for the cGMP specificity of these enzymes (model 1; Figure 4, top) (Altenhofen et al., 1991; Kumar and Weber, 1992; Weber et al., 1989). We hypothesized that cGMP is a partial agonist for SpIH because there is a valine instead of a threonine at position 621. The partial agonism could arise if the hydrogen bond between the threonine and the guanine ring of cGMP were directly involved in stabilizing the allosteric conformational change in the CNBD. Alternatively, it could arise if the hydrogen bond were required to force the cGMP into the *syn* configuration, and in that configuration cGMP was a more effective agonist.

To test the hypothesis that the threonine-to-valine change is responsible for the partial agonism of cGMP on SpIH, we mutated V621 in the wild-type SpIH channel to a threonine (V621T) and recorded the functional behavior of the mutant channels in inside-out patches from *Xenopus* oocytes. Surprisingly, the mutation had no effect on the partial agonist behavior of cGMP. As for wild-type SpIH channels, saturating cGMP still activated about half of the current activated by cAMP (for V621T, I_{cGMP}/I_{cAMP} = 0.49 ± 0.025, n = 6; for WT, I_{cGMP}/I_{cAMP} = 0.51 ± 0.035, n = 8) (Figure 4A; Table 2). The mutation also had little or no effect on voltage dependence (Figure 4B; Table 1). However, V621T did have a large effect on the apparent affinity for cGMP. The mutation caused more than a 10-fold increase in the apparent affinity for cGMP (for V621T, $K_{1/2}$ = 34.2 ± 2.5 μM, n = 6; for WT, $K_{1/2}$ = 479 ± 59.5 μM, n = 6) but little or no effect on the apparent affinity for cAMP (Figure 4C; Table 2). The results suggest that the mutant threonine is able to form a specific hydrogen bond with the guanine ring of cGMP that it cannot form with cAMP.

The effect of the V621T mutation is exclusively on the apparent affinity of the channel for cGMP, not on the

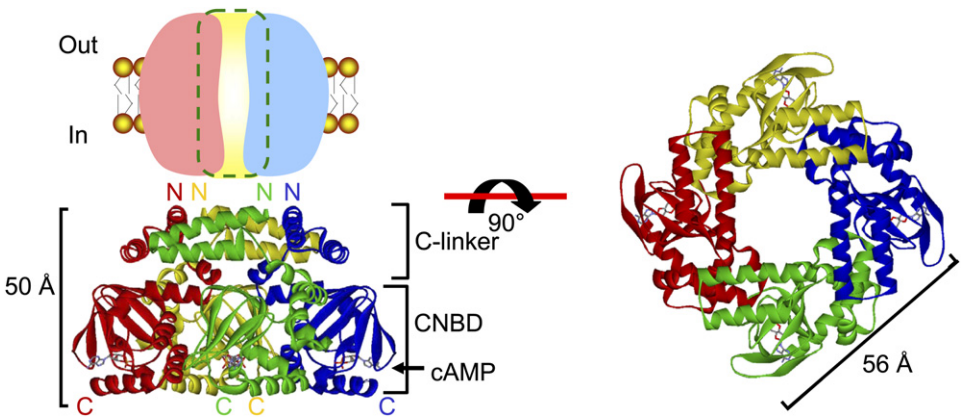

Figure 2. Structure of the SpIH Carboxy-Terminal Tetramer Bound to cAMP
SpIH tetramer viewed perpendicular (left) and parallel (right) to the four-fold axis. Each subunit is shown in a different color. Cyclic-AMP is shown as a stick model located in the CNBD.

Table 4. Summary of Crystallographic Refinement Statistics

	SpIH	HCN2-I636D
Space group	$P42_12$	I4
Resolution (Å)	65.9–1.93	500–2.25
R_{work} (%)[a]	18.7	20.8
R_{free} (%)[a]	24.2	26.1
Twinning fraction		0.43
Overall B value (Å^2)	30.4	29.0
Rmsd bond length (Å)	0.005	0.0105
Rmsd bond angle (°)	0.63	1.37

[a] $R_{work} = \Sigma_{hkl} ||F_o| - |F_c||/\Sigma_{hkl} |F_o|$, where F_o and F_c are observed and calculated structure factors, respectively; 10% of data was set aside for calculation of R_{free}.

efficacy of cGMP. The absence of an effect on the efficacy indicates that the mutation had no effect on the free energy of the opening conformational change. The increase in the apparent affinity, therefore, must be due to an increase in the affinity of binding of cGMP. These results, then, suggest that a hydrogen bond between the threonine and cGMP is involved in cGMP binding but does not change during the allosteric transition in the CNBD. Therefore, this substitution alone cannot explain the partial agonist behavior of cGMP in SpIH. Furthermore, the results suggest that the *syn* configuration of cGMP, required for the formation of the hydrogen bond, is not sufficient to make cGMP a full agonist.

An alternative model for the molecular mechanism for cGMP specificity was proposed for CNG channels (model 2; Figure 5, top) (Varnum et al., 1995). In this model, the specificity arises from specific hydrogen bonds between an aspartate in the C helix (D604 in CNGA1) and the N1 and N2 nitrogens of the guanine ring of cGMP. These hydrogen donors are not present in the adenine ring of cAMP. Furthermore, it was proposed that these interactions with cGMP form during the allosteric transition in the CNBD, not during the binding to the closed state, thus stabilizing the allosteric conformational change in the CNBD.

We therefore hypothesized that an aspartate at an equivalent position in the C helix of SpIH (I665D) would hydrogen bond with cGMP and, in turn, stabilize the allosteric conformational change in the CNBD, making cGMP a full agonist. To test this hypothesis, we measured the functional effects of the mutation I665D. Once again, the mutation did not increase the cGMP efficacy. In fact, I665D caused a significant decrease in the maximum current activated by cGMP relative to the current activated by cAMP (I_{cGMP}/I_{cAMP} = 0.09 ± 0.02, n = 6) (Figure 5A; Table 2). This was coupled with a decrease in the open

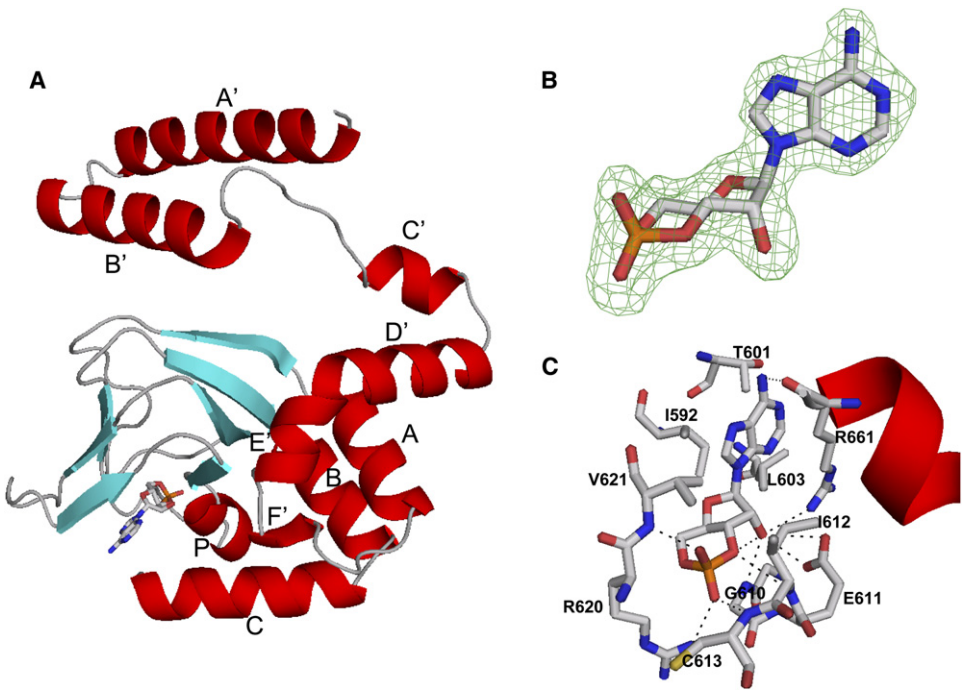

Figure 3. Summary of the Structure of a Single SpIH Subunit Bound to cAMP

(A) Ribbon representation of a single subunit showing cAMP bound between the β roll (blue) and C helix.

(B) Structure and electron density map (simulated annealing $F_o - F_c$ omit map contoured to level 2.5) of cAMP bound to SpIH. cAMP binds in the *anti* configuration.

(C) Binding interactions between SpIH and cAMP are indicated by dashed lines.

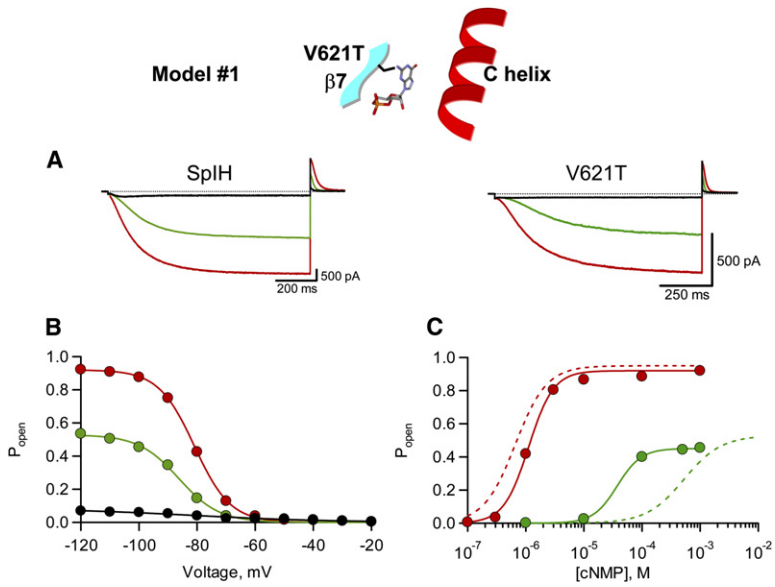

Figure 4. Functional Properties of SpIH-V621T Channels

(A) Currents from wild-type SpIH (left) and SpIH-V621T (right) channels recorded in the inside-out configuration in the absence of cyclic nucleotide (black) or the presence of 1 mM cAMP (red) or 1 mM cGMP (green). Voltage steps to −120 mV were applied, followed by steps to +30 mV.

(B) Voltage dependence of SpIH-V621T channels. Open probabilities are shown for channels in the same patch in the absence (black) or presence of cAMP (red) or cGMP (green). The smooth lines are fits of the Boltzmann function to the data. For this patch, in cAMP, $V_{1/2}$ = −81 mV; zδ = 4.1, and in cGMP, $V_{1/2}$ = −86 mV; zδ = 3.7.

(C) Dose-response relationships for SpIH-V621T channels. Open probabilities are shown for different concentrations of cAMP (red) and cGMP (green) and fit by a Hill equation. For this patch, cAMP had a $K_{1/2}$ = 1.1 μM and a Hill Coef = 2.0, while cGMP had a $K_{1/2}$ = 37.5 μM and a Hill Coef = 2.1. Dashed lines are reproduced Hill equations fit to wild-type SpIH data from Figure 1.

probability with saturating cAMP and a decrease in the apparent affinity for both cAMP and cGMP (Figure 5C; Table 2). As before, there was no effect of the mutation on the voltage dependence of activation (Figure 5B; Table 1). These results suggest that the I665D mutation caused a large destabilization of the allosteric conformational change in the CNBD for both cGMP and cAMP. A destabilization of the allosteric transition alone can largely account for both the decrease in the open probability with saturating cyclic nucleotide and the decrease in the apparent affinity of the channel for cyclic nucleotide (Colquhoun, 1998). Clearly, an aspartate in the C helix is not sufficient by itself to increase cGMP efficacy in SpIH.

As both previous models fail to account for the partial agonism of cGMP in SpIH, we considered a third model to produce cGMP specificity (model 3; Figure 6, top). In this new model, cGMP can only interact with an aspartate in the C helix when it is in the *syn* configuration. So, to obtain cGMP specificity, a threonine in the β roll is required to hold the cGMP in the *syn* configuration during binding,

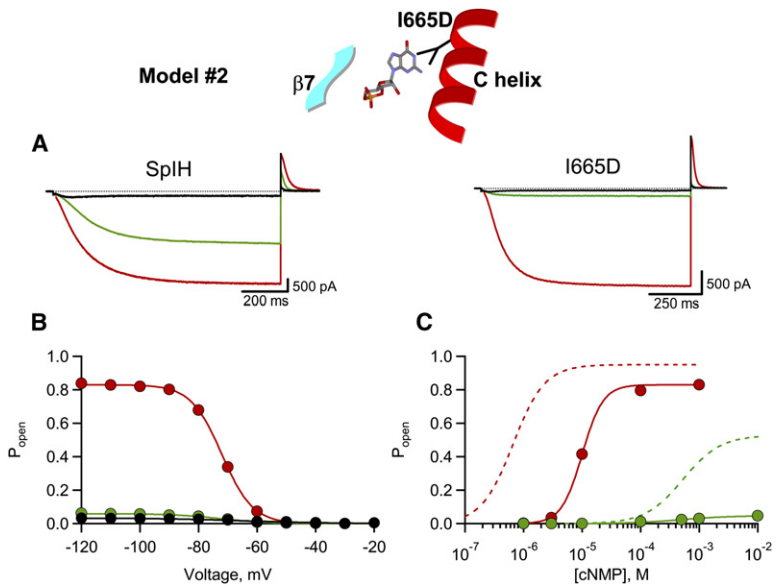

Figure 5. Functional Properties of SpIH-I665D Channels

(A) Currents from wild-type SpIH (left) and SpIH-I665D (right) channels recorded in the inside-out configuration in the absence of cyclic nucleotide (black) or the presence of 1 mM cAMP (red) or 1 mM cGMP (green). Voltage steps to −120 mV were applied, followed by steps to +30 mV.

(B) Voltage dependence of SpIH-I665D channels. Open probabilities are shown for channels in the same patch in the absence (black) or presence of cAMP (red) or cGMP (green). The smooth lines are fits of the Boltzmann function to the data. For this patch, in cAMP, $V_{1/2}$ = −72 mV; zδ = 4.9, and in cGMP, $V_{1/2}$ = −72 mV; zδ = 3.1.

(C) Dose-response relationships for SpIH-I665D channels. Open probabilities are shown for different concentrations of cAMP (red) and cGMP (green) and fit by a Hill equation. For this patch, cAMP had a $K_{1/2}$ = 10 μM and a Hill Coef = 2.2, while cGMP had a $K_{1/2}$ = 473 μM and a Hill Coef = 1. Dashed lines are reproduced Hill equations fit to wild-type SpIH data from Figure 1.

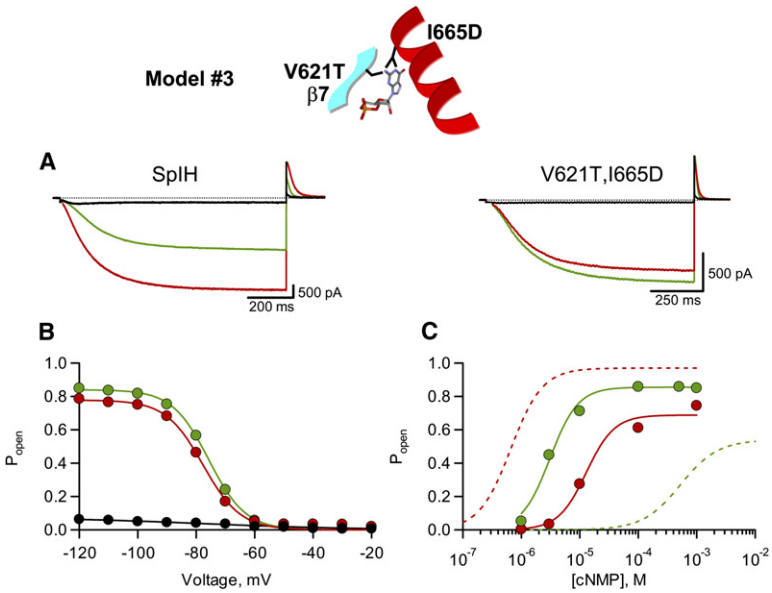

Figure 6. Functional Properties of SpIH-V621T,I665D Channels

(A) Currents from wild-type SpIH (left) and SpIH-V621T,I665D (right) channels recorded in the inside-out configuration in the absence of cyclic nucleotide (black) or the presence of 1 mM cAMP (red) or 1 mM cGMP (green). Voltage steps to −120 mV were applied, followed by steps to +30 mV.

(B) Voltage dependence of SpIH-V621T,I665D channels. Open probabilities are shown for channels in the same patch in the absence (black) or presence of cAMP (red) or cGMP (green). The smooth lines are fits of the Boltzmann function to the data. For this patch, in cAMP, $V_{1/2}$ = −78 mV; zδ = 4.4, and in cGMP, $V_{1/2}$ = −76 mV; zδ = 4.0.

(C) Dose-response relationships for SpIH-V621T,I665D channels. Open probabilities are shown for different concentrations of cAMP (red) and cGMP (green) and fit by a Hill equation. For this patch, cAMP had a $K_{1/2}$ = 20 μM and a Hill Coef = 1.1, while cGMP had a $K_{1/2}$ = 31 μM and a Hill Coef = 1.8. Dashed lines are reproduced Hill equations fit to wild-type SpIH data from Figure 1.

and an aspartate in the C helix is required to interact with the guanine ring during the allosteric transition. This model predicts that the double mutant V621T,I665D should then exhibit enhanced activation by cGMP. Figure 6 shows that this is indeed the case. In V621T,I665D channels, cGMP activated an even larger current than cAMP (I_{cGMP}/I_{cAMP} = 1.23 ± 0.06, n = 6) (Figure 6A). The open probability in the presence of saturating cGMP (0.84 ± 0.06, n = 3) and the apparent affinity for cGMP ($K_{1/2}$ = 4.3 ± 1.2 μM, n = 6) are higher than for both the wild-type and the single-mutant channels (Figure 6C; Table 2). Additionally, because both mutants are required to enhance cGMP efficacy, the new model predicts that the effects of the mutants will be highly nonadditive. A thermodynamic mutant cycle analysis revealed that the coupling energy between mutations at V621 and I665 for cGMP is −5.2 ± 0.27 kcal/mol, while for cAMP it is only −0.31 ± 0.52 kcal/mol (Figure S2). This large coupling energy seen for cGMP is normally reserved for residues that directly interact (Frisch et al., 1997; Vaughan et al., 2002). However, in this case, the coupling arises through an intermediary cGMP molecule whose configuration (*syn* versus *anti*) is affected by the V621T mutation.

Molecular Mechanism for cGMP Specificity

To fully establish the molecular mechanism for enhanced cGMP efficacy, we turned again to X-ray crystallography. Whereas previously we could not obtain cocrystals of SpIH and cGMP, we were able to obtain cocrystals of SpIH-V621T,I665D and cGMP. Unfortunately, SpIH-V621T,I665D crystals diffracted poorly (4 Å resolution) and were not suitable to observe the molecular interactions we propose above. We therefore turned to HCN2 channels. Like SpIH, HCN2 channels are activated with a higher apparent affinity for cAMP than cGMP (Figures 7A and 7C). However, for HCN2 channels, both cAMP and cGMP are full agonists and shift the voltage dependence of activation to a similar extent (Figure 7B). Importantly, similar mutations made in HCN2 also increase the cGMP specificity of the channel (Figures 7A and 7C). Like in SpIH, HCN2-I636D (HCN2 already has a threonine, T592, at the equivalent SpIH position of V621T) caused an increase in the apparent affinity for cGMP and a decrease in the apparent affinity for cAMP (Figure 7C). Together with the amino acid similarity between HCN2 and SpIH, these results strongly suggest that the mechanisms for the allosteric conformational change in the CNBD and for cGMP specificity are going to be conserved between the two channels.

The HCN2-I636D carboxy-terminal domain produced well-diffracting cocrystals with cGMP. The structure of the mutant carboxy-terminal fragment, with bound cGMP, was solved by molecular replacement to 2.25 Å resolution (Figure 8; Table 4). Overall, the backbone structure was very similar to the wild-type HCN2 and SpIH structures (rmsd of Cα atoms of 0.74 Å for HCN2 and 0.99 Å for SpIH). Differences with the wild-type HCN2 and SpIH structures, however, become apparent in the CNBD. Unlike cAMP, cGMP is bound in the *syn* configuration. This configuration permits T592 to hydrogen bond with the N2 amine of the guanine ring (Figure 8). A similar interaction was also seen in the wild-type HCN2 structure (Zagotta et al., 2003). However, in HCN2-I636D, there is a novel interaction between I636D and the guanine ring of cGMP. The carboxylate of I636D forms a new pair of hydrogen bonds with the N1 and N2 positions of the guanine ring (Figure 8). This interaction was clearly visible in both subunits in the asymmetric unit. Our functional measurements on SpIH wild-type and mutant channels indicate that this interaction is dynamic and occurs only during

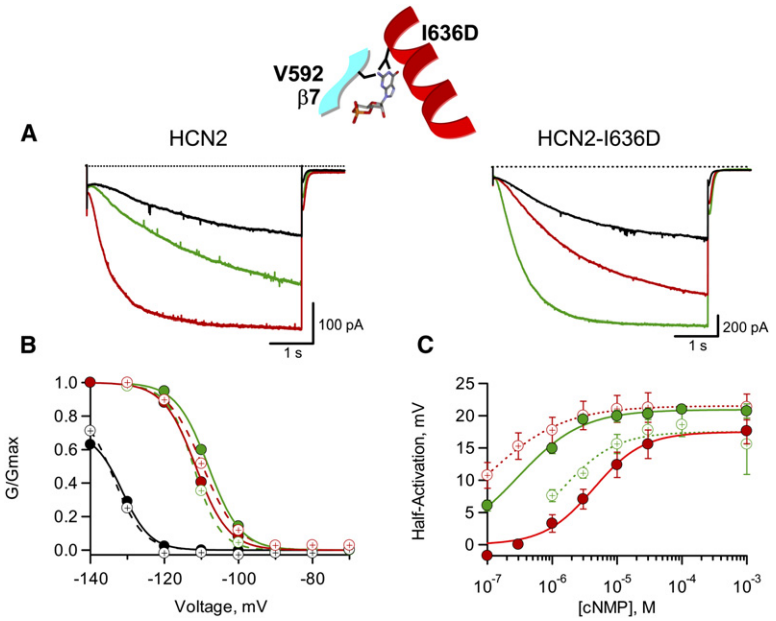

Figure 7. Functional Properties of HCN2 and HCN2-I636D Channels

(A) Currents from HCN2 (left) and HCN2-I636D (right) channels recorded in the inside-out configuration in the absence of cyclic nucleotide (black) or the presence of 1 μM cAMP (red) or 1 μM cGMP (green). Voltage steps to −130 mV were applied, followed by steps to −40 mV.

(B) Voltage dependence of HCN2-I636D channels (filled symbols) compared to HCN2 channels (open symbols). Conductance-voltage relationships are shown for channels in the same patch in the absence (black) or presence of cAMP (red) or cGMP (green). The smooth lines are fits of the Boltzmann function to the data from an HCN2-I636D patch, in cAMP (red), $V_{1/2}$ = −111 mV; zδ = 4.4, in cGMP (green), $V_{1/2}$ = −108 mV; zδ = 4.4, and in 0 cNMP (black), $V_{1/2}$ = −131 mV; zδ = 3.7. The dashed lines are fits of the Boltzmann function to the data from an HCN2 patch, in cAMP, $V_{1/2}$ = −109 mV; zδ = 4.8, in cGMP, $V_{1/2}$ = −112 mV; zδ = 3.6, and in 0 cNMP, $V_{1/2}$ = −133 mV; zδ = 4. Symbols and error bars represent mean ± SEM with n > 3.

(C) Dose-response relationships for HCN2 (open symbols) and HCN2-I636D (filled symbols) channels. Average shifts in $V_{1/2}$ are shown for three patches under different concentrations of cAMP (red) and cGMP (green). The smooth and dashed lines are fits of the Hill equation. For the HCN2-I636D patch, the average shift in cAMP had a $K_{1/2}$ = 4.4 μM and a Hill Coef = 1.1, while cGMP had a $K_{1/2}$ = 0.29 μM and a Hill Coef = 0.9. For HCN2, the average shift in cAMP had a $K_{1/2}$ = 0.09 μM and a Hill Coef = 0.7, while cGMP had a $K_{1/2}$ = 1.4 μM and a Hill Coef = 1.1. Symbols and error bars represent mean ± SEM with n > 3.

the allosteric transition. The energy of these hydrogen bonds, then, provides much of the energy that promotes channel opening.

DISCUSSION

This paper unites structural and functional evidence into a simple allosteric mechanism for cyclic nucleotide-regulated channels and enzymes. As discussed below, the results elaborate a mechanism for the allosteric conformational change in the CNBD, a mechanism for partial agonist action, and a mechanism for cGMP specificity.

Our structure of the CNBD of SpIH is similar to that of other cyclic nucleotide-binding proteins such as the cAMP-dependent protein kinase regulatory subunit (Su et al., 1995), CAP (Weber et al., 1987), a bacterial cyclic nucleotide-regulated potassium channel (Clayton et al., 2004), and HCN2 (Zagotta et al., 2003). The cyclic nucleotide is bound at the interface between the β roll and the C helix. We show in SpIH that a mutation in the β roll, V621T, specifically affects the binding of cyclic nucleotides, whereas a mutation in the C helix, I665D, affects the allosteric transition. These results suggest an allosteric mechanism where the cyclic nucleotide initially docks with the β roll (Figure 9). Then, coupled to the opening conformational change in the channel, there is an allosteric conformational change in the CNBD that moves the C helix into position to interact with the purine ring of the cyclic nucleotide. The energy of these interactions between the C helix and the purine ring is harvested to drive the opening conformational change in the channel pore. A similar mechanism has been proposed for the CNBD of other cyclic nucleotide-regulated enzymes (Clayton et al., 2004; Lee et al., 1994; Rehmann et al., 2003; Varnum et al., 1995; Vigil et al., 2006).

From our experiments, we can also gain insights into the mechanisms of partial agonism in general. Previously, two molecular mechanisms have been proposed for partial agonist action. In the classic mechanism, partial agonism arises from incomplete stabilization of the allosteric conformational change in the ligand binding site (Li et al., 1997; Monod et al., 1965). Therefore, whereas for this mechanism the conformational change is identical for full and partial agonists, its equilibrium is more favorable for full agonists than for partial agonists. In another mechanism, exemplified by the AMPA subtype of glutamate receptors (Mayer and Armstrong, 2004), partial agonist action is produced by a smaller or different conformational change in the ligand binding site. We show with both structural and functional experiments that a mutation that provides new interactions between cGMP and the C helix specifically converts cGMP into a full agonist. These results suggest that cGMP is a partial agonist in wild-type channels because it is unable to sufficiently stabilize movement of the C helix, which is coupled to the opening conformational change in the channel pore, thus consistent with the classic mechanism. Another possible explanation is that the partial agonist action of cGMP arises because the C helix is in a different conformation with cGMP bound than with cAMP bound, and the mutation causes the C helix to adopt a cAMP-like configuration when cGMP is bound.

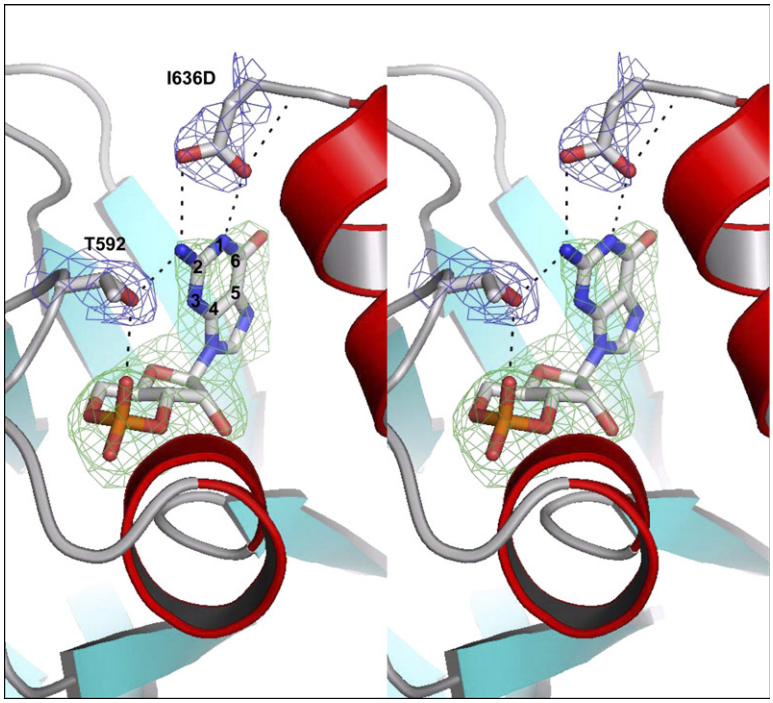

Figure 8. Interactions of cGMP with T592 of the β Roll and I636D of the C Helix

Stereo view showing cGMP in the *syn* configuration bound to HCN2-I636D. A simulated annealing $F_o - F_c$ omit map (green) is shown for cGMP and a $2F_o - F_c$ omit map (blue) is shown for T592 and I636D. Dashed lines indicate hydrogen-bonding interactions between the N2 amine of the guanine ring and T592 and between the N1 and N2 amines of the guanine ring and the carboxylate group of I636D.

Finally, our experiments establish, to our knowledge for the first time, the molecular mechanism for cGMP specificity in some cyclic nucleotide-regulated channels and enzymes such as CNG channels and cGMP-dependent protein kinases. Previously, two models for cGMP specificity have been proposed. In model 1 (Figure 4, top), the specificity arises from specific interactions between a threonine in the β roll and the N2 amine of cGMP (Altenhofen et al., 1991; Kumar and Weber, 1992; Scott et al., 1996; Weber et al., 1989). This interaction could only occur if cGMP were in the *syn* configuration. In model 2 (Figure 5, top), the specificity arises from interactions between an aspartate in the C helix and the N1 and N2 nitrogens of cGMP (Varnum et al., 1995). Based on modeling using the structure of CAP, this interaction was thought to only occur if cGMP was in the *anti* configuration. Here we show that the truth lies somewhere in between (model 3; Figure 6, top). The cGMP is held in the *syn* configuration by interactions with the threonine in the β roll, but this interaction is not sufficient to promote opening by cGMP. Instead, interactions with an aspartate in the C helix promote opening by cGMP. Because of differences in the position of the C helix between the HCN/SpIH structures and CAP, the specific interaction between cGMP and the aspartate actually occurs only when cGMP is in the *syn* rather than the *anti* configuration. This mechanism, ironically unraveled in a mutant cAMP-gated channel, likely applies to cGMP-gated channels and cGMP-regulated enzymes, which also have a threonine in the β roll and an acidic residue in the C helix.

If an acidic residue in the C helix is required for cGMP to be a full agonist for SpIH, why is cGMP a full agonist for HCN2 (which contains an isoleucine at the equivalent position in the C helix)? We speculate that the opening allosteric conformational change in HCN2 is just less energetically costly than that in SpIH. Therefore, existing

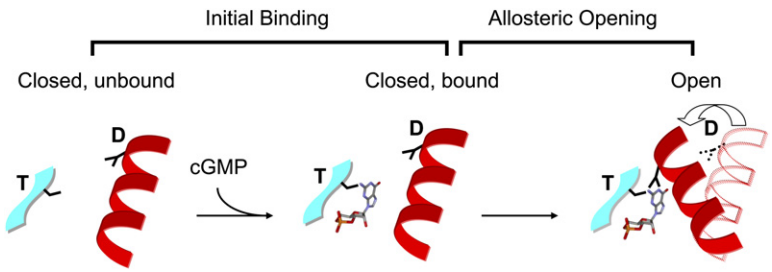

Figure 9. Molecular Mechanism for Conformational Changes Occurring in the CNBD

Model of the cGMP binding and conformational rearrangement that lead to activation of the SpIH channel. The ligand binds to the closed channel primarily through interactions between the β roll and the ribose and phosphate of the cyclic nucleotide. For cGMP, threonine in the β roll plays an important roll in stabilizing cGMP in the *syn* configuration. The opening allosteric conformational change involves the movement of the C helix relative to the β roll. For cGMP, aspartate in the β roll stabilizes the rearrangement, promoting channel opening.

interactions between cGMP and the C helix are sufficient to promote the conformational change without additional interactions from the aspartic acid. A similar explanation has been shown to underlie why cAMP is a partial agonist in the rod CNG channel (CNGA1) but a full agonist in the olfactory CNG channel (CNGA2) (Gordon and Zagotta, 1995). Overall, these results highlight the many commonalities in the mechanisms of regulation of different cyclic nucleotide-regulated effector proteins.

EXPERIMENTAL PROCEDURES

DNA Preparation for Physiology

SpIH cDNA (a gift from U.B. Kaupp) was subcloned into the pGEMHE high-expression vector (a gift from E. Liman), where it is flanked by the 5′ and 3′ *Xenopus* β-globin gene UTR. Mouse HCN2 cDNA (a gift from S. Siegelbaum) was in the pGEM vector. All cDNAs were linearized and then transcribed in vitro using the Ambion T7 Message Machine into mRNAs. The mRNA was injected into surgically isolated stage IV *Xenopus* oocytes as previously described (Zagotta et al., 1989). All mutations were generated using oligonucleotide-directed PCR mutagenesis and confirmed with fluorescence-based DNA sequencing.

Electrophysiology

Electrophysiology experiments were conducted on full-length SpIH or SpIH mutant channels exogenously expressed in plasma membranes of *Xenopus* oocytes. SpIH channels were recorded in excised inside-out macropatches using conventional patch-clamp recording techniques (Hamill et al., 1981). Both pipette and bath solutions contained 130 mM KCl, 0.2 mM EDTA, and 3 mM HEPES (pH 7.2). Currents were elicited by applying a series of voltage test pulses (range of −10 to −120 mV in −10 mV increments) followed by a constant +30 mV tail pulse. We calculated the open probability (P_o) from tail current amplitudes by subtracting steady-state tail currents, normalizing to a maximum of 1, then multiplying by the $P_{o,max}$ determined from noise analysis. The P_o versus voltage data were fit with the Boltzmann equation: $P_o = P_{o,max}/(1 + e^{[-z\delta(V - V_{1/2})F/RT]})$, where V is the pulse voltage, $V_{1/2}$ is the activation midpoint voltage, and zδ is the equivalent charge movement. All fitting was performed with Igor software (Wavemetrics). Data parameters were expressed as mean ± SEM and tabulated for comparison.

Ligand specificity of SpIH and mutant channels was examined by comparing dose-response relationships for cAMP and cGMP. Cyclic-AMP or cGMP was applied to the cytoplasmic side of inside-out patches using a gravity-controlled perfusion system (RSC-100; BioLogic). Data for dose-response relationships taken at saturating negative voltages (−100 mV) were normalized to $P_{o,max}$ determined from nonstationary noise analysis and fit with the Hill equation: $P_o = P_{o,max}/(1 + (K_{1/2}/[A])^h)$, where [A] is the agonist concentration, $K_{1/2}$ is the agonist concentration eliciting half-maximal response, and h is the Hill coefficient. Data parameters were expressed as mean ± SEM and tabulated for comparison.

Nonstationary noise analysis was performed on current traces elicited by applying 1 s pulses to −130 mV to patches in the presence of 1 mM cAMP or 1 mM cGMP applied to the cytoplasmic side of patches. The mean and variance of the corresponding points of a sequential pair of current traces were calculated using a pairwise subtraction method (Heinemann and Conti, 1992). The variance was plotted relative to the mean and data were fit with a parabolic function: variance = base + $Ii - I^2/N$, where I is the mean current, base is the baseline noise, *i* is the single-channel current, and N is the number of channels. A maximum open probability was calculated from the equation $P_{o,max} = I_{max}/Ni$. The single-channel conductance, γ, was calculated using the equation $\gamma = i/V$, where V is the voltage during the hyperpolarizing step.

Protein Preparation for Crystallography

The DNA fragment encoding amino acid residues 470–665 of SpIH was cloned into pHMalc2T, a derivative of pMalc2T (New England Biolabs) containing a hexahistidine tag at the N terminus of the maltose-binding protein (MBP). This construct was transformed into *Escherichia coli* BL-21(DE3) cells and induced as previously described (Zagotta et al., 2003). The cells were collected by centrifugation and resuspended in ice-cold lysis buffer (30 mM HEPES, 500 mM NaCl, 10% glycerol, 10 μM cAMP, 1 mM β -mercaptoethanol, 0.1 mM phenylmethylsulfonyl chloride, and 2.5 μg/ml DNase [pH 7.5]). The cells were then lysed in an Emulsiflex-C5 (Avestin), and the lysate was cleared by centrifugation. The SpIH-MBP fusion protein was purified on a 100 ml amylose affinity column (New England Biolabs) and eluted with 50 mM maltose. The glycerol concentration was then increased to 30%, and MBP was removed by thrombin cleavage and separated by Ni2-NTA chromatography. The HCN2-I636D construct encoding amino acids 443–640 of HCN2 was purified essentially the same as described above except the lysis buffer contained 150 mM NaCl instead of 500 mM NaCl.

Crystallization and Structure Determination

Protein fragments of the SpIH carboxy-terminal region were concentrated to 10–20 mg/ml in the presence of 5 mM cAMP. Cocrystals of SpIH and cAMP were grown using the hanging drop method. Essentially, 1 μl of protein solution containing 10 mM hexamine cobalt trichloride was mixed with 1 μl of reservoir solution containing 10% (w/v) PEG 6000, 0.5 M NaCl, 20% glycerol, and 0.1 M HEPES (pH 8). These conditions produced tetragonal crystals with space group $P42_12$ that diffracted to a resolution of 1.9 Å. Crystals were flash-frozen in liquid nitrogen. Diffraction data were collected at beamline X4A at the National Synchrotron Light Source. Integration, scaling, and merging of the diffraction data were done with the HKL suite of programs (http://www.hkl-xray.com). Structures were determined by molecular replacement using AMoRe software (CCP4, 1994) and existing HCN2 carboxy-terminal structures as search probes. Models of the SpIH carboxy-terminal region were built using the software program O (Jones and Kjeldgaard, 1997) and $2F_o - F_c$ omit maps. Refinement of the models was done with CNS (Brunger et al., 1998). Parameters used to define the stereochemistry of cAMP and cGMP were derived from the corresponding small-molecule crystal structures obtained from the Cambridge Structure Database (http://www.ccdc.cam.ac.uk).

The cocrystals of HCN2-I636D and cGMP were grown using a similar protocol except hexamine cobalt trichloride was not added to the protein solution, and the reservoir solution contained 10% (w/v) PEG 8000, 0.5 M NaCl, 15% glycerol, and 0.1 M MES (pH 5). These conditions produced tetragonal crystals with space group I4 that diffracted to a resolution of 2.25 Å. Diffraction data were collected at beamline 8.2.1 at Advanced Light Source. Integration, scaling, and merging of the diffraction data were done as described above. An analysis of the intensity statistics carried out by Xtriage of the PHENIX suite (Adams et al., 2004) indicated that the data were merohedrally twinned with twin law (-k,-h,-l). The twin fraction was estimated to be equal to 0.43. The structure was solved via the molecular replacement method, using the program MOLREP (Vagin and Teplyakov, 1997) and the structure of Protein Data Bank ID code 1Q3E as a search model. The model was subjected to refinement using the amplitude-based least-squares target function in CNS that takes into account twinning. Model rebuilding was carried out with Coot (Emsley and Cowtan, 2004), guided by results of the validation program MolProbity (Davis et al., 2004). The data processing and refinement statistics are given in Table 4 and Table S1, respectively.

Supplemental Data

Supplemental Data include two figures and one table and can be found with this article online at http://www.structure.org/cgi/content/full/15/6/671/DC1/.

ACKNOWLEDGMENTS

We are grateful to Heidi Utsugi, Shellee Cunnington, and Gay Sheridan for technical assistance. We thank Nelson Olivier and Eric Gouaux for helpful discussions. X-ray diffraction data sets were collected at NSLS and ALS, and we thank the beamline personnel for their assistance. We thank Tinatin Brelidze, Anne Carlson, Kimberley Craven, Sharona Gordon, Michael Puljung, Noah Shuart, and Justin Taraska for comments on the manuscript. This work was supported by the Howard Hughes Medical Institute and a grant from the National Eye Institute (EY10329) to W.N.Z.

Received: January 17, 2007
Revised: April 9, 2007
Accepted: April 20, 2007
Published: June 12, 2007

REFERENCES

Adams, P.D., Gopal, K., Grosse-Kunstleve, R.W., Hung, L.W., Ioerger, T.R., McCoy, A.J., Moriarty, N.W., Pai, R.K., Read, R.J., Romo, T.D., et al. (2004). Recent developments in the PHENIX software for automated crystallographic structure determination. J. Synchrotron Radiat. *11*, 53–55.

Altenhofen, W., Ludwig, J., Eismann, E., Kraus, W., Bonigk, W., and Kaupp, U.B. (1991). Control of ligand specificity in cyclic nucleotide-gated channels from rod photoreceptors and olfactory epithelium. Proc. Natl. Acad. Sci. USA *88*, 9868–9872.

Altomare, C., Bucchi, A., Camatini, E., Baruscotti, M., Viscomi, C., Moroni, A., and DiFrancesco, D. (2001). Integrated allosteric model of voltage gating of HCN channels. J. Gen. Physiol. *117*, 519–532.

Baruscotti, M., and Difrancesco, D. (2004). Pacemaker channels. Ann. N Y Acad. Sci. *1015*, 111–121.

Biel, M., Schneider, A., and Wahl, C. (2002). Cardiac HCN channels: structure, function, and modulation. Trends Cardiovasc. Med. *12*, 206–212.

Brunger, A.T., Adams, P.D., Clore, G.M., DeLano, W.L., Gros, P., Grosse-Kunstleve, R.W., Jiang, J.S., Kuszewski, J., Nilges, M., Pannu, N.S., et al. (1998). Crystallography & NMR System: a new software suite for macromolecular structure determination. Acta Crystallogr. D Biol. Crystallogr. *54*, 905–921.

CCP4 (Collaborative Computational Project, Number 4) (1994). The CCP4 suite: programs for X-ray crystallography. Acta Crystallogr. D Biol. Crystallogr. *50*, 760–763.

Clayton, G.M., Silverman, W.R., Heginbotham, L., and Morais-Cabral, J.H. (2004). Structural basis of ligand activation in a cyclic nucleotide regulated potassium channel. Cell *119*, 615–627.

Colquhoun, D. (1998). Binding, gating, affinity and efficacy: the interpretation of structure-activity relationships for agonists and of the effects of mutating receptors. Br. J. Pharmacol. *125*, 924–947.

Craven, K.B., and Zagotta, W.N. (2004). Salt bridges and gating in the COOH-terminal region of HCN2 and CNGA1 channels. J. Gen. Physiol. *124*, 663–677.

Davis, I.W., Murray, L.W., Richardson, J.S., and Richardson, D.C. (2004). MolProbity: structure validation and all-atom contact analysis for nucleic acids and their complexes. Nucleic Acids Res. *32*, W615–W619.

Del Castillo, J., and Katz, B. (1957). Interaction at end-plate receptors between different choline derivatives. Proc. R. Soc. Lond. B Biol. Sci. *146*, 369–381.

DiFrancesco, D. (1991). The contribution of the 'pacemaker' current (if) to generation of spontaneous activity in rabbit sino-atrial node myocytes. J. Physiol. *434*, 23–40.

DiFrancesco, D., Ducouret, P., and Robinson, R.B. (1989). Muscarinic modulation of cardiac rate at low acetylcholine concentrations. Science *243*, 669–671.

Emsley, P., and Cowtan, K. (2004). Coot: model-building tools for molecular graphics. Acta Crystallogr. D Biol. Crystallogr. *60*, 2126–2132.

Frisch, C., Schreiber, G., Johnson, C.M., and Fersht, A.R. (1997). Thermodynamics of the interaction of barnase and barstar: changes in free energy versus changes in enthalpy on mutation. J. Mol. Biol. *267*, 696–706.

Gauss, R., Seifert, R., and Kaupp, U.B. (1998). Molecular identification of a hyperpolarization-activated channel in sea urchin sperm. Nature *393*, 583–587.

Gordon, S.E., and Zagotta, W.N. (1995). Localization of regions affecting an allosteric transition in cyclic nucleotide-activated channels. Neuron *14*, 857–864.

Hamill, O.P., Marty, A., Neher, E., Sakmann, B., and Sigworth, F.J. (1981). Improved patch-clamp techniques for high-resolution current recording from cells and cell-free membrane patches. Pflugers Arch. *391*, 85–100.

Heinemann, S.H., and Conti, F. (1992). Nonstationary noise analysis and application to patch clamp recordings. Methods Enzymol. *207*, 131–148.

Jones, T., and Kjeldgaard, M. (1997). Electron-density map interpretation. Methods Enzymol. *277*, 173–208.

Kaupp, U.B., and Seifert, R. (2001). Molecular diversity of pacemaker ion channels. Annu. Rev. Physiol. *63*, 235–257.

Kumar, V.D., and Weber, I.T. (1992). Molecular model of the cyclic GMP-binding domain of the cyclic GMP-gated ion channel. Biochemistry *31*, 4643–4649.

Lee, E.J., Glasgow, J., Leu, S.F., Belduz, A.O., and Harman, J.G. (1994). Mutagenesis of the cyclic AMP receptor protein of *Escherichia coli*: targeting positions 83, 127 and 128 of the cyclic nucleotide binding pocket. Nucleic Acids Res. *22*, 2894–2901.

Li, J., Zagotta, W.N., and Lester, H.A. (1997). Cyclic nucleotide-gated channels: structural basis of ligand efficacy and allosteric modulation. Q. Rev. Biophys. *30*, 177–193.

Mayer, M.L., and Armstrong, N. (2004). Structure and function of glutamate receptor ion channels. Annu. Rev. Physiol. *66*, 161–181.

Monod, J., Wyman, J., and Changeux, J.P. (1965). On the nature of allosteric transitions: a plausible model. J. Mol. Biol. *12*, 88–118.

Pape, H.C. (1996). Queer current and pacemaker: the hyperpolarization-activated cation current in neurons. Annu. Rev. Physiol. *58*, 299–327.

Rehmann, H., Prakash, B., Wolf, E., Rueppel, A., De Rooij, J., Bos, J.L., and Wittinghofer, A. (2003). Structure and regulation of the cAMP-binding domains of Epac2. Nat. Struct. Biol. *10*, 26–32.

Robinson, R.B., and Siegelbaum, S.A. (2003). Hyperpolarization-activated cation currents: from molecules to physiological function. Annu. Rev. Physiol. *65*, 453–480.

Scott, S.P., Harrison, R.W., Weber, I.T., and Tanaka, J.C. (1996). Predicted ligand interactions of 3′5′-cyclic nucleotide-gated channel binding sites: comparison of retina and olfactory binding site models. Protein Eng. *9*, 333–344.

Shin, K.S., Maertens, C., Proenza, C., Rothberg, B.S., and Yellen, G. (2004). Inactivation in HCN channels results from reclosure of the activation gate: desensitization to voltage. Neuron *41*, 737–744.

Su, Y., Dostmann, W.R., Herberg, F.W., Durick, K., Xuong, N.H., Ten Eyck, L., Taylor, S.S., and Varughese, K.I. (1995). Regulatory subunit of protein kinase A: structure of deletion mutant with cAMP binding domains. Science *269*, 807–813.

Vagin, A., and Teplyakov, A. (1997). MOLREP: an automated program for molecular replacement. J. Appl. Cryst. *30*, 1022–1025.

Varnum, M.D., Black, K.D., and Zagotta, W.N. (1995). Molecular mechanism for ligand discrimination of cyclic nucleotide-gated channels. Neuron *15*, 619–625.

Vaughan, C.K., Harryson, P., Buckle, A.M., and Fersht, A.R. (2002). A structural double-mutant cycle: estimating the strength of a buried salt bridge in barnase. Acta Crystallogr. D Biol. Crystallogr. *58*, 591–600.

Vigil, D., Lin, J.H., Sotriffer, C.A., Pennypacker, J.K., McCammon, J.A., and Taylor, S.S. (2006). A simple electrostatic switch important in the activation of type I protein kinase A by cyclic AMP. Protein Sci. *15*, 113–121.

Weber, I.T., Gilliland, G.L., Harman, J.G., and Peterkofsky, A. (1987). Crystal structure of a cyclic AMP-independent mutant of catabolite gene activator protein. J. Biol. Chem. *262*, 5630–5636.

Weber, I.T., Shabb, J.B., and Corbin, J.D. (1989). Predicted structures of the cGMP binding domains of the cGMP-dependent protein kinase: a key alanine/threonine difference in evolutionary divergence of cAMP and cGMP binding sites. Biochemistry *28*, 6122–6127.

Zagotta, W.N., Hoshi, T., and Aldrich, R.W. (1989). Gating of single Shaker potassium channels in *Drosophila* muscle and in *Xenopus* oocytes injected with Shaker mRNA. Proc. Natl. Acad. Sci. USA *86*, 7243–7247.

Zagotta, W.N., Olivier, N.B., Black, K.D., Young, E.C., Olson, R., and Gouaux, E. (2003). Structural basis for modulation and agonist specificity of HCN pacemaker channels. Nature *425*, 200–205.

Accession Numbers

The structures of SpIH and HCN2-I636D have been deposited in the Protein Data Bank under ID codes 2PTM and 2Q0A.

